Acta Materialia 124 (2017) 456–467

Contents lists available at ScienceDirect

Acta Materialia

journal homepage: www.elsevier.com/locate/actamat

Full length article

Precipitation strengthening and reversed yield stress asymmetry in Mg alloys containing rare-earth elements: A quantitative study

P. Hidalgo-Manrique [a, *], J.D. Robson [b], M.T. Pérez-Prado [a]

[a] IMDEA Materials Institute, C/Eric Kandel 2, 28906, Getafe, Madrid, Spain
[b] School of Materials, University of Manchester, MSS Tower, Manchester, M13 9PL, UK

ARTICLE INFO

Article history:
Received 30 July 2016
Received in revised form
23 September 2016
Accepted 6 November 2016
Available online 19 November 2016

Keywords:
Magnesium-rare earth alloys
Precipitation
Orowan strengthening
Reversed yield stress asymmetry
High temperature

ABSTRACT

The effect of prismatic plates on the mechanical behaviour at low and high temperature of a Mg-1 wt.% Mn- 1 wt%Nd alloy was determined. For this purpose, a weakly textured extruded bar, exhibiting similar values for the critical resolved shear stresses of the various deformation systems, was annealed at 275 °C for different time periods. During these thermal treatments the grain size and texture remained invariant, but different precipitate distributions, characterised by transmission electron microscopy (TEM), were generated. The as-extruded and the annealed material were tested under tension and compression at room temperature (RT) and 250 °C along the extrusion direction. Precipitation was observed to harden the alloy at RT and to induce a reversed yield stress (YS) asymmetry, the compressive YS being higher than the tensile YS. At 250 °C, the alloy is anomalously resistant under compressive conditions, exhibiting an enhanced reversed YS asymmetry. In order to assess the strengthening effect of particles on the individual major Mg deformation systems, appropriate versions of the Orowan equation were developed. The correlation of the predicted results with the experimental data revealed that reversed YS asymmetry at RT is attributable to a strong promotion of prismatic slip over twinning. Finally, experimental observations by TEM suggested that reversed YS asymmetry at high temperature arises from a different interaction of pyramidal <c+a> dislocations with particles and solutes in tension and compression.

1. Introduction

Magnesium (Mg), as the lightest engineering material, is a preferable material for lightweight applications, its alloys having a great potential for material substitution in automotive, aerospace and other industries [1]. Plastic deformation in Mg is accomplished by the activation of certain slip and twin systems. Slip may take place along the $<11\bar{2}0>$ or <a> direction mainly on the basal {0002} and first order prismatic $\{10\bar{1}0\}$ planes and along the $<11\bar{2}3>$ or <c+a> direction on the second order pyramidal planes $\{11\bar{2}2\}$ planes [2,3], while twinning occurs predominantly on the pyramidal $\{10\bar{1}2\}$ planes [4,5]. Due to the low symmetry of the hexagonal closed packed structure and the associated lack of sufficient independent slip systems, the mechanical properties of Mg are highly dependent on the crystallographic orientation [6]. This mechanical anisotropy is further accentuated by the polar nature of twinning, additionally leading to a large dependence on the deformation mode (tension, compression) or mechanical asymmetry [3,5]. Moreover, the ease of activation of the various deformation systems is actually determined by their critical resolved shear stresses, whose values are influenced by testing conditions [7,8] and microstructural features, such as grain size [9], solutes [10–12] or precipitates [13–31]. Therefore, the mechanical response of Mg alloys can be controlled by changing the microstructure, irrespectively of the texture and the deformation mode. In this sense, precipitation has been recognised as an important tool for controlling the strength of the individual slip and twin modes.

The precipitates that typically form in Mg alloys have the shape of rods or plates lying on particular crystallographic planes [23]. It is known that the strength of Mg alloys is affected not only by the particle volume fraction, but also by the shape and orientation of particles [16,20,23,28,30,31]. For example, in randomly textured materials, the strength achievable when basal plates form, as is the

* Corresponding author. Present address: School of Materials, University of Manchester, MSS Tower, Manchester, M13 9PL, UK.
E-mail address: paloma.hidalgo-manrique@manchester.ac.uk (P. Hidalgo-Manrique).

http://dx.doi.org/10.1016/j.actamat.2016.11.019

case of Mg-Al-Zn (AZ) alloys, is generally lower than when prismatic plates form, as in Mg-Y-RE (rare-earth) alloys [20,28]. This difference may be at least partly attributed to the different Orowan hardening of basal slip, the most easily activated deformation mode in Mg, due to the different interparticle spacing produced by the same volume fraction of different precipitate shapes and habits. In fact, the Orowan increment of the critical resolved shear stress (τ) for basal slip produced by prismatic plates is larger than that produced by equivalent volume fractions of basal plates, c-axis rods or spherical particles [16,20,23,28,31].

It is also known that particles of different shape and habit strengthen the different deformation modes to different extents [17–20,22,25–27,29,31]. As a consequence, the usually undesirable room temperature (RT) mechanical anisotropy and asymmetry usually observed in the Mg wrought products are also affected by the shape and orientation of particles. For example, the precipitation of basal plates in the AZ91 alloy reduces the yield stress (YS) asymmetry along the extrusion direction (ED), whereas the presence of c-axis rods in the Z5 leads to an increase in the YS asymmetry along ED. It has been suggested that the ratio of the increase in τ for twinning to that for prismatic slip is the key parameter determining whether precipitation will increase or reduce asymmetry of strongly textured Mg alloys [18,20,24,27,28].

Although the shape and orientation of precipitate particles have been long recognised as potentially important factors in determining the mechanical behaviour of Mg alloys, their quantitative effects on the individual slip and twinning systems of precipitation-hardened alloys have received relatively reduced attention [16–26,28–31]. In the case of slip, there is fairly good agreement between strengthening by the Orowan mechanism, based on the bowing of dislocations around particles, and the experimental data. Thus, Orowan equations appropriate for Mg alloys strengthened by rationally-oriented, shear-resistant precipitate plates and rods have been developed for basal and prismatic slip [16,17,19,20,22,23,26,28,31] and very recently also for pyramidal <c+a> slip [31], the only slip mechanism which allows the grains with the hardest orientation to deform plastically. However, although several studies have shown a strong influence of precipitates on twinning in Mg alloys, the mechanisms by which twinning dislocations interact with particles are far less clear than the interaction of slip dislocations with precipitates. In fact, unlike slip, the classical Orowan model does not fully account for the hardening of the twin system produced by precipitates [20,22,28], which must have additional contributions from other deformation mechanisms. In particular, the back stress arising from the elastic deformation of particles has been recently proved to play a significant role on the strengthening of the twinning system [30].

It is known from several experimental studies that particles can indeed have a strong effect on twinning in magnesium [13–15,20,22,27,28]. Twinning involves nucleation and growth and precipitates will influence both processes. Experimentally, it has been demonstrated in a number of precipitate containing magnesium alloy systems that particles lead to narrower twins, but do not prevent twin nucleation [17–19,24]. Indeed, while the volume fraction of twins can decrease [17,18] or remain invariant [19,24], when particles are present an increased number of smaller twins are usually observed, even for lamellar precipitate structures [24]. Therefore, although changes in the critical stress for nucleation have not been entirely ruled out, it is usually considered that the additional stress for twin growth is the critical factor in determining the strengthening against twinning. In this sense, three different behaviours have been observed when growing twins interact with particles in magnesium alloys, depending on the relative dimension of the twin and the precipitate [15]. In particular, large particles can often completely arrest twin growth, with twinning usually continuing by nucleation of a new twin in the matrix on the far side of the particle [28], while small particles can either become engulfed by a growing twin without shearing themselves [14,17,19,20,22,28,29] or can be sheared inside the twins [13,21,30].

Conventional Mg alloys soften at about 120 °C to 150 °C [32,33]. Improving the elevated temperature mechanical properties has become a critical issue to enable applications of Mg alloys at higher temperatures. One way to enable high temperature operation is by adding RE elements to Mg in order to form thermally stable Mg-RE precipitates, which can also act as effective obstacles for dislocation slip at elevated temperatures. Despite the large potential for extending the strengthening effect of particles to higher temperatures and thereby increasing the maximum service temperature, the incidence of precipitates on the mechanical behaviour of Mg-RE alloys at moderate temperatures has not been extensively explored. A few studies [34,35] suggest that the manifestation in these alloys of an unexpected reversed YS asymmetry at such temperatures, with the compressive YS being higher than the tensile YS when testing along the extrusion direction (ED), could be related to the asymmetric nature of the interaction between dislocations and particles or solutes. However, additional efforts are still required to fully elucidate the fundamental mechanisms underlying such phenomenon.

This paper is aimed at quantifying the strengthening effect of different distributions of prismatic plates on the Mg major deformation systems at low and high temperature and to relate this to the mechanical behaviour of particle-containing Mg-RE alloys. For this purpose, an extruded MN11 alloy, containing Nd, was annealed at 275 °C up to different time intervals ranging from 0.5 h to 20 h. Both the as-extruded and the annealed samples were tested under tension and compression along ED at RT and 250 °C. A detailed quantitative TEM analysis has been utilised to characterise the precipitate distribution in the annealed samples and the interaction of particles with dislocations. Finally, appropriate versions of the Orowan equation for the major Mg deformation systems were developed, these being validated by comparing the predicted results and the experimental data.

2. Experimental procedure

The material under study is a Mg MN11 alloy with chemical composition (wt.%) 1 Mn, 1 Nd, Mg (balance). Billets for extrusion produced by gravity casting were machined up to a diameter of 93 mm. The billets were homogenised at 350 °C during 15 h before extrusion. Indirect extrusion was carried out at 300 °C and 5.5 mm/s to produce round bars of 17 mm in diameter, which corresponds to an extrusion ratio of 1:30.

The as-extruded material was annealed at 275 °C for 0.5, 1, 5 and 20 h and quenched in water immediately afterwards. Samples for thermal treatments were encapsulated in Pyrex tubes filled with Ar atmosphere.

Tensile and compressive specimens were electrodischarge machined from the as-extruded and the annealed bars with their loading axis parallel to ED. The tensile specimens had a cylindrical geometry with a gauge section of 4 mm in diameter and 12 mm in length. The compressive specimens were also cylindrical with 3 mm in diameter and 4.5 mm in height. Uniaxial tensile and compressive tests were performed at RT and 250 °C using a Servosis universal testing machine equipped with an elliptical furnace with four quartz lamps in air. The specimens were pulled to failure with a constant rate of crosshead displacement giving an initial strain rate of 10^{-3} s^{-1}. Prior to testing at 250 °C, the specimens were kept for 5 min at such temperature and, upon completion of the tests, the specimens were immediately water-cooled to preserve the

microstructure. The testing temperature was measured with the aid of a thermocouple clamped close to the specimens. The compression tests were performed using lubrication in order to minimise friction between the sample and the anvils. The YS corresponding to each test was calculated as the true stress at 0.2% engineering strain.

Microstructural examinations were performed by means of optical microscopy (OM) in an Olympus BX-51 microscope, scanning electron microscopy (SEM) in a FEI Helios NanoLab 600i field emission gun microscope and transmission electron microscopy (TEM) at an accelerating voltage of 200 kV in a JEOL JEM 2100 microscope. The macrotexture was analysed by XRD. The (0001), $(10\bar{1}0)$, $(10\bar{1}1)$, $(10\bar{1}2)$, $(10\bar{1}3)$ and $(11\bar{2}0)$ pole figures were measured using Cu K_α radiation in a X'Pert PRO ALPHA1 PANalytical diffractometer furnished with a PW3050/60 goniometer. From these experimental data, the orientation distribution function (ODF) and the calculated pole figures were obtained using the MATLAB toolbox MTEX [36]. The inverse pole figures (IPFs) were then derived from the calculated direct pole figures. In preparation for OM, SEM and XRD, samples were mounted and then ground with SiC papers and polished with diamond pastes down to a 1 μm finish. In addition, the specimens for OM were chemically etched in an acetic picral solution to reveal the grain boundaries, while the specimens for SEM were final polished in colloidal silica. Thin foils for TEM were cut perpendicular to the extrusion or the testing direction, punched into discs of 3 mm in diameter, mechanically ground to 50 μm in thickness and then ion milled to perforation using a Gatan Precision Ion Polishing System.

3. Results and discussion

3.1. Microstructural evolution with annealing

Fig. 1 illustrates the inverse pole figure in the ED of the as-extruded bar as well as OM micrographs from the cross sections of the as-extruded bar and from the samples annealed for 1 and 20 h. The average grain size, measured by the linear intercept method, has been added as an inset to each micrograph. Although there is a depletion of orientations in the vicinity of the <0001> pole (Fig. 1a), the as-extruded bar exhibits a very broad angular distribution of the ED and thus displays a very weak texture whose maximum intensity is only 2.6 times random. This weak texture, contrasting with the typical strong prismatic $<10\bar{1}0>$ fibre or $<10\bar{1}0>-<11\bar{2}0>$ double fibre textures exhibited by the extruded bars of conventional Mg alloys [37], has been previously attributed to specific dynamic or static recrystallization phenomena associated with nucleation at shear bands and restriction of grain growth [38]. Fig. 1b–d shows that both the as-extruded bar and the annealed samples exhibit a homogeneous and fully recrystallised microstructure composed of equiaxed grains with an average size of approximately 15 μm. The remarkable grey shading that develops within the grains of the annealed samples (Fig. 1c, d) suggests that the distribution of particles and/or solutes changes during annealing.

Figs. 2 and 3 illustrate, respectively, cross-sectional SEM and TEM images of the as-extruded material and of samples annealed for 0.5 and 20 h. The as-extruded microstructure (Figs. 2a and 3a) is populated by particles that are smaller than 100 nm in size. These particles, which are thermally stable and are located both within the grains as well as at the grain boundaries (GBs), appear in white contrast in the SEM micrographs (Fig. 2a) and in black contrast in the TEM micrographs (Fig. 3a). Their composition is close to pure Mn and they exhibit a large variety of sizes and morphologies [35,38,39]. The role of these Mn particles as inhibitors of grain boundary migration contributes, reportedly, to the invariance of the grain size of the MN11 alloy upon annealing [38]. In the as-extruded state, Nd atoms are present mostly in solid solution. However, following annealing at 275 °C (Figs. 2b, c and 3b–d) precipitation of Nd-containing plates, apparently nucleated at the Mn particles and often forming in pairs, takes place. A closer

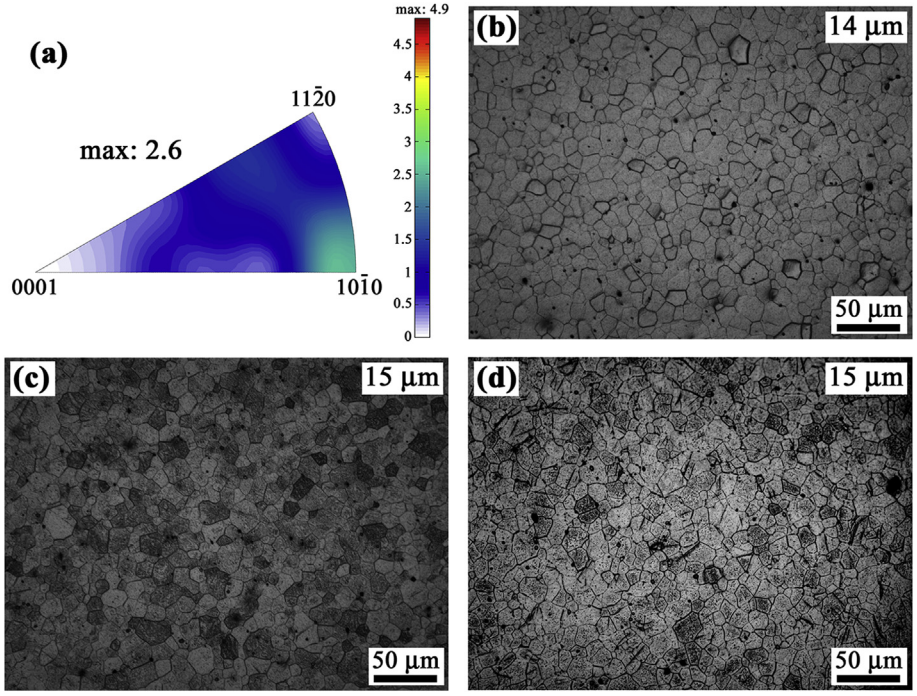

Fig. 1. (a) Inverse pole figure in the extrusion direction of the as-extruded bar and optical micrographs corresponding to the transversal section of (b) the as-extruded bar and of the samples annealed at 275 °C for (c) 1 h and (d) 20 h. The average grain size values are included as insets in the micrographs.

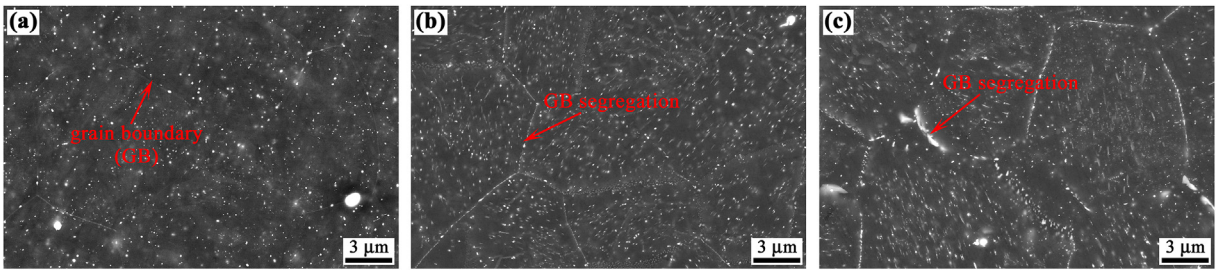

Fig. 2. SEM micrographs corresponding to the transversal section of (a) the as-extruded bar and of the samples annealed at 275 °C for (b) 0.5 h and (c) 20 h.

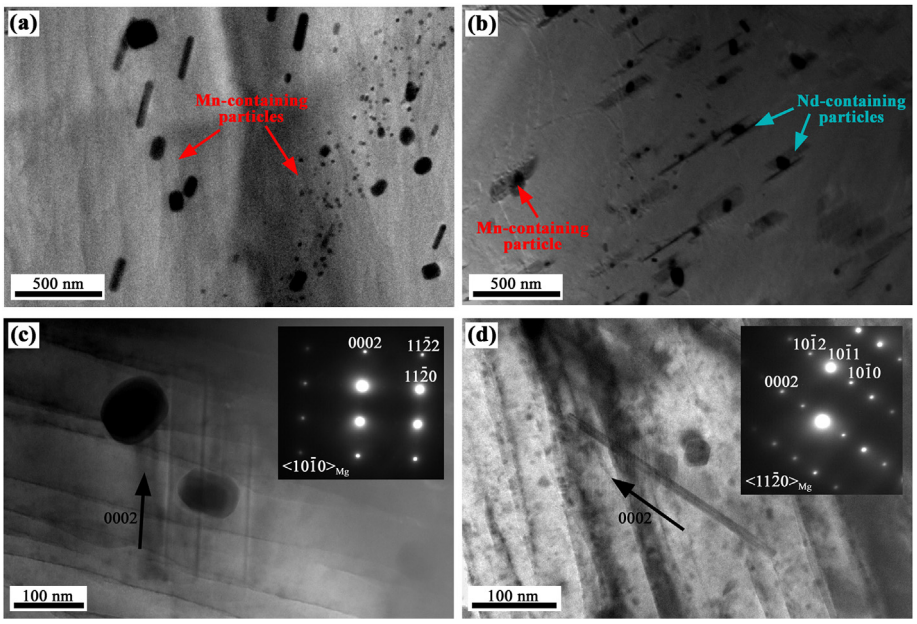

Fig. 3. TEM bright-field images showing the distribution of precipitates in (a) the as-extruded bar and (b) the sample annealed at 275 °C for 0.5 h. A more detailed view of the Nd-containing particles that precipitate during annealing is illustrated in (c,d). The electron beam is parallel to extrusion direction in (a,b), to the matrix <10$\bar{1}$0> direction in (c) and to the matrix <11$\bar{2}$0> direction in (d). The selected area diffraction patterns corresponding to the oriented grains are shown as insets.

inspection of the annealed microstructures along the <10$\bar{1}$0> (Fig. 3c) and <11$\bar{2}$0> (Fig. 3d) zone axes reveals that such particles, identified as the metastable Mg_3Nd phases [35,38,39], are plates with a prismatic {10$\bar{1}$0} habit and their longer axis parallel to the matrix [0001] direction. Additionally, in the annealed samples, GBs appear clearly decorated with particles, especially with increasing annealing time (Fig. 2b and c). This is consistent with the large tendency of the RE solute atoms to segregate to the GBs [40,41], which may also contribute to the thermal stability of the grain structure in the MN11 alloy. Finally, large insoluble constituent intermetallic particles that consist of Fe [42] were also found in both the as-extruded and the annealed states.

The mean length (l), width (w) and thickness (t) of individual prismatic plates, as well as their volume fraction (f) were measured from the TEM micrographs. More concretely, the volume fraction of Mg_3Nd particles was calculated as $(n \times V_p)/(A \times h)$ [43], where n is the number of particles in a selected area A, $V_p = l \times w \times t$ is the mean volume of individual particles and h is the specimen thickness, which was assumed to be 100 nm for all the examined region [44]. Fig. 4 illustrates the evolution of V_p, l, w, t and f versus the annealing time. It can be seen that V_p (Fig. 4a) is maximum at 0.5 h of annealing and then decreases with increasing soaking time, reaching a minimum at 5 h and increasing afterwards. f (Fig. 4b) follows the opposite trend, exhibiting a maximum at 5 h of annealing time. It is interesting to note that, the changes in V_p and thus in f can be mainly ascribed to changes in the particle length (Fig. 4a). In fact, the width and, especially, the thickness of the particles remain approximately constant even after prolonged annealing. This data reflect the coexistence of precipitation and dissolution of the Nd-containing prismatic plates at annealing times exceeding 0.5 h. When the soaking time is shorter than 5 h, precipitation processes prevail, causing f to increase despite the reduction of the volume of individual particles, which already start to dissolve; for annealing times longer than 5 h particle dissolution becomes dominant, leading to a pronounced decrease of the particle volume fraction. At this stage, coarsening of a limited number of plates and enhanced GB segregation (Fig. 2c) take place.

3.2. Room temperature mechanical behaviour

Fig. 5 depicts the mechanical response of the as-extruded and the annealed bars under tension and compression along ED at RT. The shape of the stress-strain curves (Fig. 5a, b) reveals the dominance of crystallographic slip during the first stages of deformation in tension and the occurrence of a large activity of twinning in compression. Moreover, it can be appreciated (Fig. 5c) that annealing after extrusion leads to notable increases in the tensile

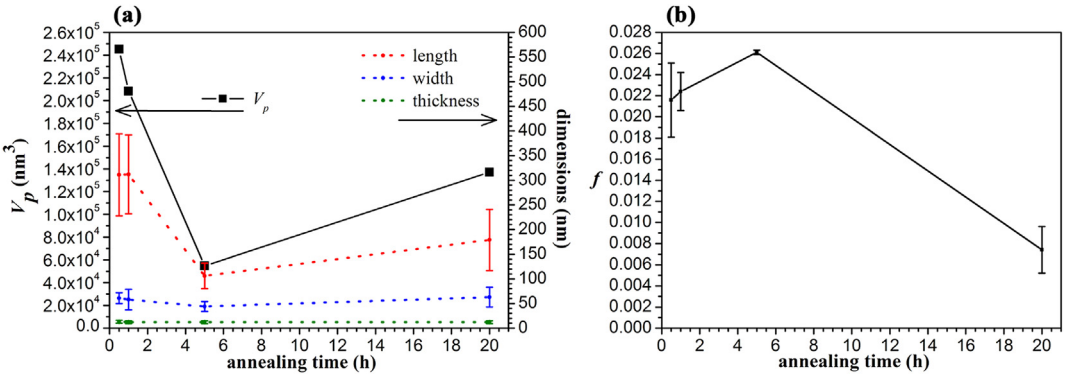

Fig. 4. (a) Volume (V_p), length, width, thickness and (b) volume fraction (f) of the plate-shaped Nd-containing particles as a function of annealing time.

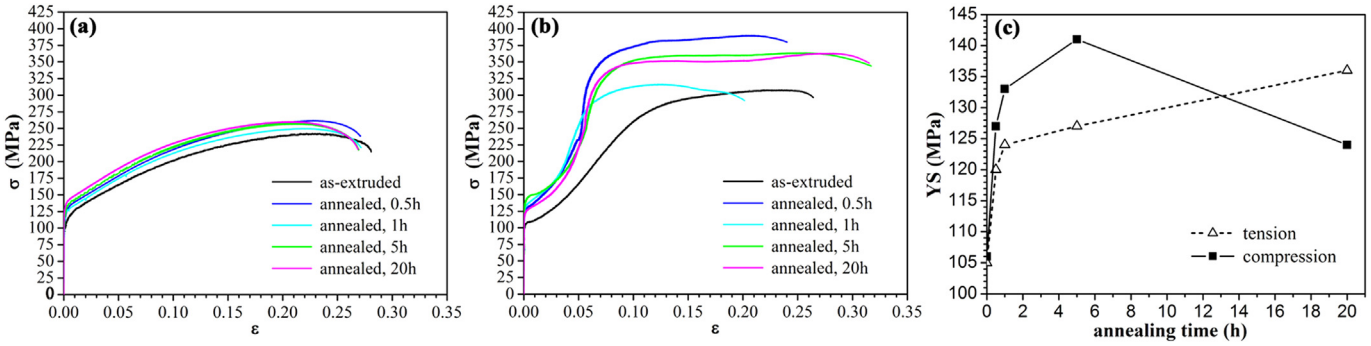

Fig. 5. Mechanical behaviour of the as-extruded and the annealed bars at RT when testing along the extrusion direction: (a) tensile curves, (b) compressive curves and (c) variation of the tensile and compressive YS with the annealing time.

and compressive YS at RT. Since the grain size and texture remain unchanged during annealing (Fig. 1), the observed strengthening can be only related to the precipitation of Nd-containing particles (Figs. 2 and 3). Finally, it is clear (Fig. 5c) that precipitation enhances the YS asymmetry. Note that, with the exception of the tests carried out in the sample annealed for 20 h, the YS asymmetry is reversed, the compressive YS being higher than the tensile YS.

3.2.1. Orowan strengthening

In order to quantify the effect of Nd-containing particles on the RT mechanical properties of the MN11 alloy, the increment in τ produced by the need for dislocations to bypass the Mg_3Nd precipitates, i.e., the Orowan strengthening ($\Delta\tau$), was estimated as follows. For point obstacles of identical strength, the Orowan increment in τ is expressed as [16,23]:

$$\Delta\tau = \frac{Gb}{2\pi\lambda\sqrt{1-\nu}}\ln\left(\frac{d_p}{r_0}\right) \quad (1)$$

where G is the shear modulus of the Mg matrix phase (16.5 GPa), b is the magnitude of the Burgers vector for the gliding dislocations in Mg, λ is the effective planar interparticle spacing on the slip or twin plane, ν is the Poisson's ratio of the Mg matrix phase (0.35), d_p is the mean planar diameter of the particles on the slip or twin plane and r_0 is the core radius of the dislocations in Mg.

The magnitude of the Burgers vector (b) is equal to a for <a> dislocations [45], and it is taken as $a/7$ for twinning dislocations [4] and as $(c^2+a^2)^{1/2}$ for <c+a> dislocations [45], where $a = 0.32$ nm and $c = 0.52$ nm are the Mg lattice parameters. The dislocation core radius (r_0) is the region around a dislocation in which the distortion is too large to be described by elasticity theory [45]. For the sake of simplicity, it has been usually assumed that $r_0 = b$. However, r_0 is actually dependant on the character of the dislocation [45]. Based on atomistic simulation studies [46–48], r_0 was determined as a for basal <a> dislocations, $3a$ for twinning dislocations, $0.35a$ for prismatic <a> dislocations and $2.6a$ for pyramidal <c+a> dislocations. Only slip screw dislocations were considered. The estimated values for b and r_0 are listed in Table 1. Note that the Burgers vector of twinning dislocations is about an order or magnitude smaller than that corresponding to slip dislocations. It is also remarkable that, the core of the twinning and the <c+a> dislocations is much more extended than that of <a> dislocations.

The mean planar diameters of the particles were calculated as $2(S_p/\pi)^{1/2}$, being S_p the average intersection area of the particles with the corresponding slip or twin plane (Fig. 6). Prismatic plates make two different intersections with twin, prismatic and pyramidal planes (S_p^1 and S_p^2), S_p taking then the value of the mean average of these two areas. Thus, the intersection areas of the particles with the various slip and twin planes can be approximated by

$$S_p^{basal} = w \times t \quad (2)$$

$$S_p^{twin} = 1.3328\ (w \times t) \quad (3)$$

$$S_p^{prism} = 0.3333\ (l \times w) + 0.7698\ (l \times t) \quad (4)$$

$$S_p^{pyr} = 1.7284\ (w \times t) \quad (5)$$

For the calculation of the effective planar interparticle spacings, the prismatic plates are assumed to have an ideal arrangement at

Table 1
Values of the Burgers vector (b) and the dislocation core radius (r_0) considered for the calculation of the Orowan stresses.

Dislocation parameter	Basal <a>	Twinning	Prismatic <a>	Pyramidal <c+a>
b (Å)	3.2	0.458	3.2	6.1
r_0 (Å)	3.2	9.6	1.1	8.3

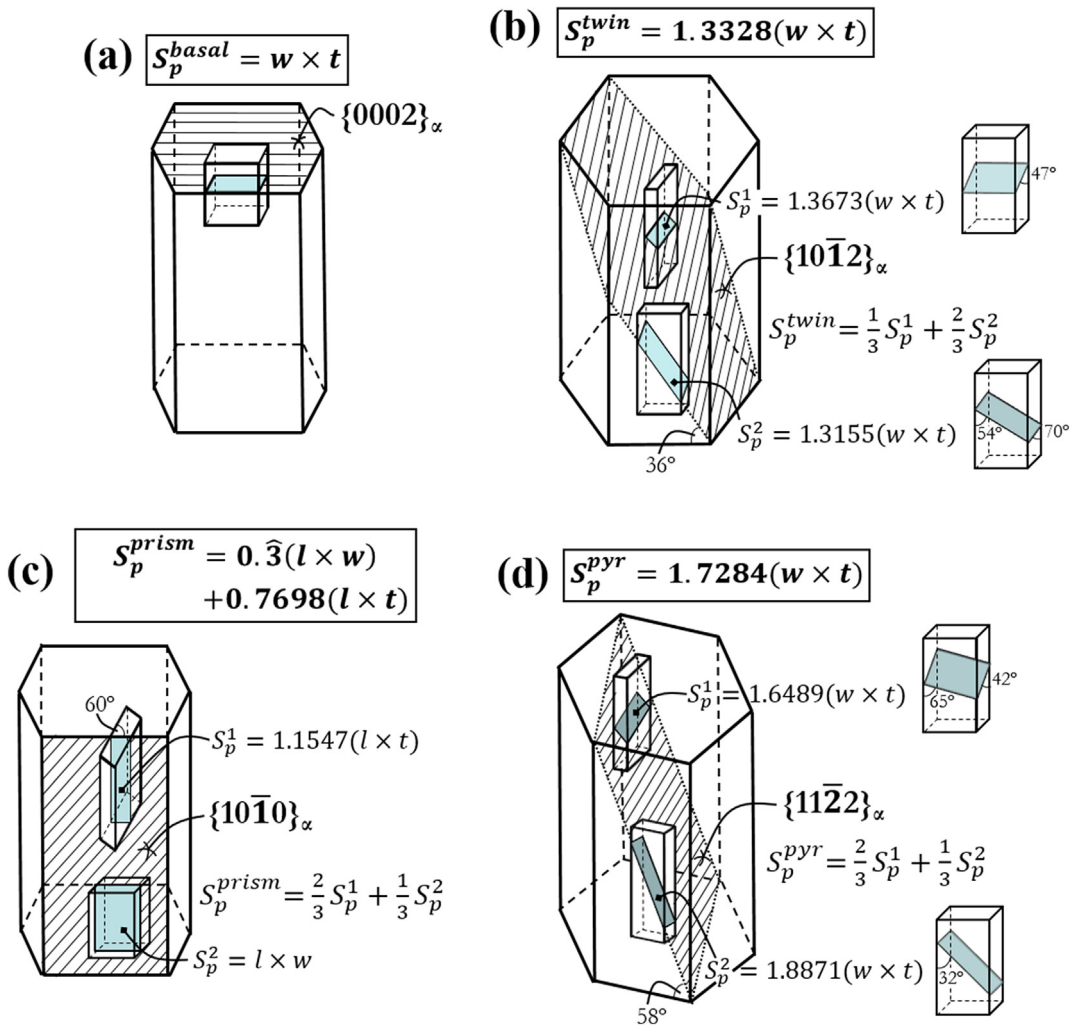

Fig. 6. Schematic diagrams showing the intersection area of the particles (S_p) with (a) basal planes, (b) twin planes, (c) prismatic planes, and (d) pyramidal planes.

the centre of each rectangular face of a triangular-based prism in the matrix phase (Fig. 7). Note that, while the major axes of the projections of the precipitates constitute an equilateral triangle on the basal planes, they constitute an isosceles triangle with a base angle of 66° and 43° on the twin and pyramidal planes, respectively, and a scalene right-angled triangle, one of the angles being 58°, on the prismatic planes. Accordingly, λ will be defined as the value of the mean average of the distances between neighbouring particles. The values of λ for the different slip and twin planes are, thus, given by

$$\lambda_{basal} = L_p^{basal} - 0.5w - 0.8660t \tag{6}$$

$$\lambda_{twin} = L_p^{twin} - 0.6093w - 0.9808t \tag{7}$$

$$\lambda_{prism} = L_p^{prism} - 0.\hat{3}l - 0.3208w - 0.7408t \tag{8}$$

$$\lambda_{pyr} = L_p^{pyr} - 0.6818w - 0.8682t \tag{9}$$

where $L_p = 1.075/\sqrt{N_a}$ on the slip or twin plane is the mean planar centre-to-centre interparticle spacing and $N_a = f/S_p$ is the number of particles per unit area of slip or twin plane. Substituing Eqs. (2)–(5) into Eqs. (6)–(9), the effective planar interparticle spacings can be rewritten as

$$\lambda_{basal} = \frac{1.075\sqrt{w \times t} - (0.5w + 0.8660t)\sqrt{f}}{\sqrt{f}} \tag{10}$$

$$\lambda_{twin} = \frac{1.2411\sqrt{w \times t} - (0.6093w + 0.9808t)\sqrt{f}}{\sqrt{f}} \quad (11)$$

$$\lambda_{prism} = \frac{0.6206\sqrt{l \times w} + 0.9432\sqrt{l \times t} - \left(0.\widehat{3}l + 0.3208w + 0.7408t\right)\sqrt{f}}{\sqrt{f}} \quad (12)$$

$$\lambda_{pyr} = \frac{1.4133\sqrt{w \times t} - (0.6818w + 0.8682t)\sqrt{f}}{\sqrt{f}} \quad (13)$$

Now, substituing Eqs. (2)–(5) and (10)–(13) into Eq. (1), the appropriate versions of the Orowan equation of the MN11 alloy for the different deformation systems, containing prismatic precipitate plates, are obtained:

$$\Delta\tau_{basal} = \frac{1042.3\sqrt{f}}{1.075\sqrt{w \times t} - (0.5w + 0.8660t)\sqrt{f}} \ln\left(1.1284\sqrt{w \times t}\right) \quad (14)$$

$$\Delta\tau_{twin} = \frac{149.2\sqrt{f}}{1.2411\sqrt{w \times t} - (0.6093w + 0.9808t)\sqrt{f}} \ln\left(1.3027\sqrt{w \times t}\right) \quad (15)$$

$$\Delta\tau_{prism} = \frac{1042.3\sqrt{f}}{0.6206\sqrt{l \times w} + 0.9432\sqrt{w \times t} - \left(0.\widehat{3}l + 0.3208w + 0.7408t\right)\sqrt{f}} \times \ln\left(1.1284\sqrt{0.\widehat{3}(w \times t) + 0.7698(l \times t)}\right) \quad (16)$$

$$\Delta\tau_{pyr} = \frac{1988.8\sqrt{f}}{1.4133\sqrt{w \times t} - (0.6818w + 0.8682t)\sqrt{f}} \ln\left(1.4948\sqrt{w \times t}\right) \quad (17)$$

Representations of d_p, λ, $\Delta\tau$ and τ for the various deformation planes and systems versus the annealing time are given in Fig. 8. The critical resolved shear stresses were calculated as $\tau_0 + \Delta\tau$, where τ_0 is the critical resolved shear stress of the alloy in the as-extruded state and whose values were previously obtained for the major Mg deformation systems by an inverse optimisation strategy based on crystal plasticity finite element simulation [49]. It can be seen that d_p exhibits, for all the slip and twin planes, a minimum value after an annealing time of 5 h (Fig. 8a). The effective planar interparticle spacings also exhibit a minimum at an annealing time of 5 h (Fig. 8b), which is consistent with the measured increase in the particle volume fraction (Fig. 4b). As a consequence, $\Delta\tau$ (Fig. 8c) and thus τ (Fig. 8d) reach (for all the deformation systems) a maximum value in the bar annealed at 275 °C for 5 h. The behaviour of the critical resolved shear stresses is consistent with the evolution of the RT tensile YS and the RT compressive YS with annealing time (Fig. 5c), suggesting that the mechanical behaviour of the annealed bars can be largely attributed to precipitation hardening.

Our results reveal that the increment in τ produced by the precipitation of the prismatic plates is comparatively much smaller on prismatic slip than on pyramidal and basal slip (Fig. 8c). The relative values of τ_{basal} and τ_{prism} are consistent with previous predictions on the hardening effect of prismatic plates against basal and prismatic slip [25,28]. Moreover, recent theoretical calculations, using Orowan equations, showed that the <c+a> systems are generally strengthened the most by prismatic precipitate plates, followed by basal and prismatic slip systems [31]. Our quantitative study, based on solid experimental measurements on the precipitate geometry and distribution over a wide range of annealing conditions, brings evidence to confirm this trend.

Fig. 8c also shows that the Orowan strengthening of the prismatic plates on the twinning dislocations is an order of magnitude lower than that corresponding to slip, which could be attributed to the small Burgers vector of the twin dislocations (Table 1). However, this is not consistent with the observed higher value of the YS in compression, where twinning prevails upon yielding, than in tension, where slip is dominant (Fig. 5c). Thus, additional precipitate strengthening contributions on twinning, other than the Orowan stress, must be considered. Indeed, a recent work by Jain et al. [30] indicates that the strengthening effect of particles on the twinning system can be mainly attributed to the associated back stresses.

3.2.2. Effect of back stress

Twins can interact with particles in a number of ways, depending on particle characteristics. For the size of particles that

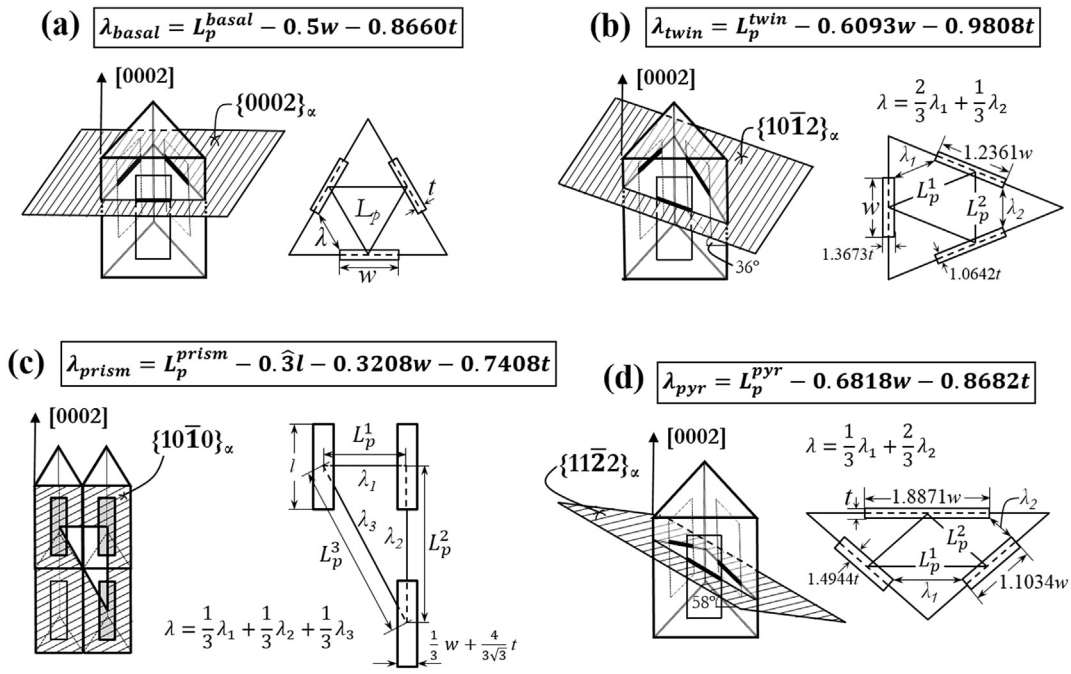

Fig. 7. Schematic diagrams showing the effective planar interparticle spacing (λ) on (a) basal planes, (b) twin planes, (c) prismatic planes and (d) pyramidal planes.

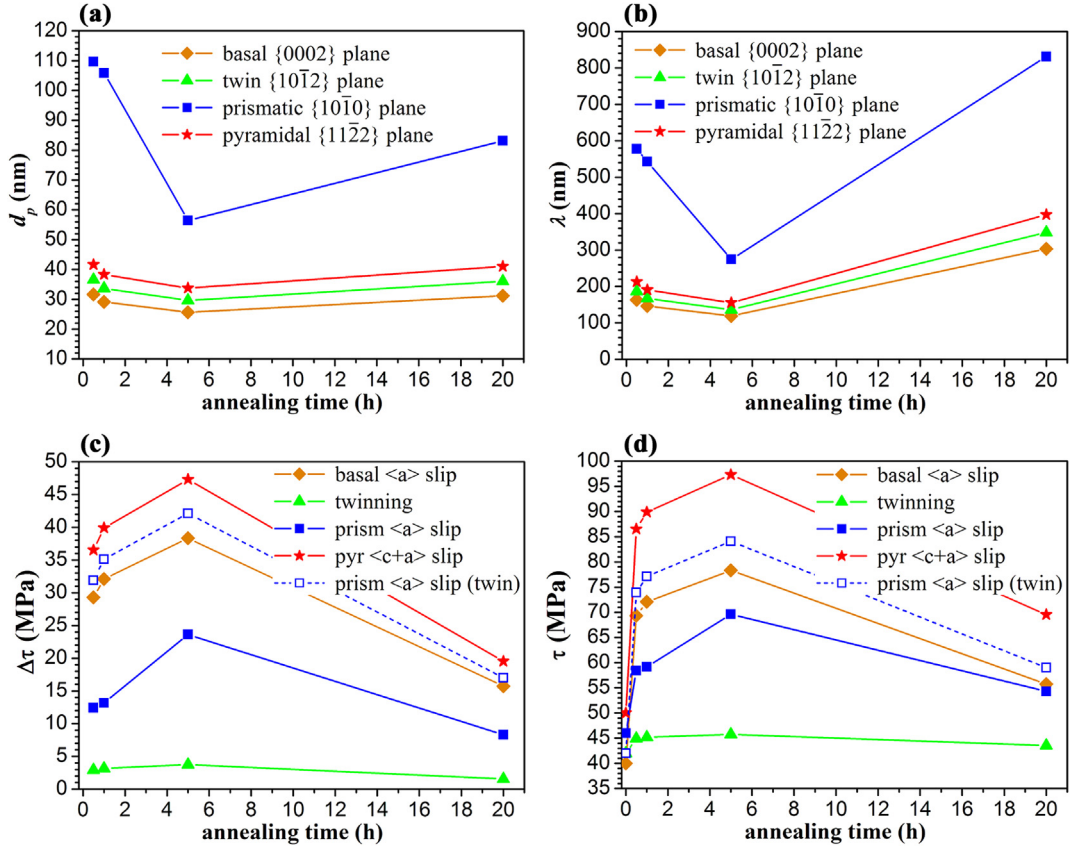

Fig. 8. Representation as a function of the annealing time of (a) the particle mean planar diameter (d_p) and (b) the effective planar interparticle spacing (λ) on the major Mg slip and twin planes; (c) the Orowan increment in the critical resolved shear stress ($\Delta\tau$) and (d) the critical resolved shear stress (τ) for all the major Mg deformation systems in the parent plus for prismatic slip in the twin.

achieves a maximum in the strengthening response during ageing, particles have been observed to become fully engulfed by a growing twin, leading ultimately to particle rotation, but not to particle shearing [14,17,19,20,22,28,29]. When the precipitates are not sheared in the twin, whereas the matrix is, a plastic strain discontinuity at the particle-matrix interface is created. This means that a back-stress or uniform mean stress that opposes the stress causing deformation in the matrix is generated. This is an additional contribution to the overall back-stress that acts on the twin. In order for the twin to keep growing in the absence of particle shear, the back-stress caused by particles must be relieved. Plastic deformation by slip plays an important role in moderating the strain discontinuity around particles in the twin, a role that is controlled by the level of slip inhibition in the twin or, in other words, by the resistance provided by particles to plastic deformation in the twin. Note that since the matrix is rotated 86° by twinning, the effectiveness of particles in strengthening slip in the twin will be different to that in the parent material. If the particles in the twin are highly effective in inhibiting slip, then less plastic relaxation can occur and hence higher back-stress levels will be retained, leading to an increment in the stress required for continued twin growth.

In the particle-containing MN11 alloy under investigation, the critical resolved shear stress for prismatic slip is significantly smaller than that corresponding to other slip modes (Fig. 8d). Therefore, it can be assumed that prismatic slip will be responsible for most of the plastic deformation necessary to moderate the strain incompatibility between particles and the matrix in the twin. Accordingly, the Orowan stress for twinning can be estimated as the Orowan stress for prismatic slip in the twin. Note that the effect of reorientation of the lattice by twinning is that 1/3 of the prismatic plates in the parent lie on basal planes in the twin and 2/3 of the prismatic plates in the parent lie on pyramidal planes in the twin. The Orowan strengthening against prismatic slip in the twin ($\Delta\tau_{prism(twin)}$) is represented in Fig. 8c, which illustrates that the reorientation of the matrix in the twin has a large incidence on the strengthening contribution of the precipitates. It is clearly seen that prismatic plates strengthen more effectively against prismatic slip in the twin than in the matrix. Indeed, the strengthening produced by prismatic plates on prismatic slip in the twin and thus on twinning is very similar to that produced on basal slip in the parent. This is due to the fact that they are in a better orientation to intersect prismatic planes and thus to block prismatic slip in the twin than in the parent. The representation of τ_{prism} in the twin (hereafter called τ'_{twin}) in Fig. 8d indicates that, when considering the effect of the back-stress, the values of the critical resolved shear stress for twinning in the particle-containing material are actually very close to those for τ_{basal} and significantly higher than those for τ_{prism} (Fig. 8d).

3.2.3. Reversed yield stress asymmetry

Extruded commercial Mg alloys are usually affected by undesirable RT yield stress asymmetry, the compressive YS being typically as little as half the tensile YS when tested along ED [50]. One of the contributors to this phenomenon is the development of strong prismatic fibre textures during extrusion and subsequent annealing, with basal {0001} planes being parallel to ED [37]. The other contributor is the polar nature of mechanical twinning [4,5]. Twinning along the $\{10\bar{1}2\}$ planes is active only when the deformation conditions are such that an extension along the c-axis takes place. Accordingly, when loading along ED in compression, the microstructure is well aligned for deformation twinning [51]. On the contrary, in tension, the twins cannot activate and instead the deformation is dominated by prismatic slip [51]. At RT the twinning system is relatively soft compared to slip [7,8]. Consequently, the compressive YS is lower than the tensile YS.

As mentioned, the as-extruded material in the present work does not exhibit at RT any tension-compression YS asymmetry (Fig. 5c). This result could be attributed to the texture weakening effect of Nd (Fig. 1) since a broader distribution of basal planes would favour the predominance of basal slip under both tension and compression along ED [50]. However, besides weakening texture, Nd additions cause the critical resolved shear stresses for all the deformation systems to become very similar (Fig. 8d), which could be ascribed to the anisotropic hardening effect of the Nd solute atoms [35,49]. This is also consistent with the absence of mechanical asymmetry in the as-extruded material for the reason that it would result in a promotion of non-basal slip at the expense of twinning.

The development of a reversed YS asymmetry observed in the annealed samples cannot be explained by changes in the grain size or texture, which remain unchanged (Fig. 1). Instead, alterations of the relative critical resolved shear stresses with respect to the as-extruded state are required to explain it. It has been suggested that, in weakly textured Mg alloys, the onset of a reversed YS asymmetry requires a marked reduction in τ_{prism} relative to τ_{twin} [52]. Our results reveal, indeed, a significant decrease of the τ_{prism}/τ_{twin} ratio in the annealed samples in which a pronounced reversed yield stress asymmetry was observed.

In Table 2, the calculated values for the τ_{prism}/τ_{twin}, τ_{pyr}/τ'_{twin} and $\tau_{basal}/\tau'_{twin}$ ratios are compiled. This data reveal that the $\tau_{prism}/\tau'_{twin}$ ratio decreases with precipitation, in particular from a value of 1.10 in the as-extruded material to values of 0.77 and 0.83 in the samples annealed for 1 h and 5 h, respectively. The τ_{pyr}/τ'_{twin} and $\tau_{basal}/\tau'_{twin}$, on the contrary, remain invariant for all the conditions (1.17 and 0.94, respectively). In the sample annealed for 20 h, where a direct yield stress asymmetry is observed, the $\tau_{prism}/\tau'_{twin}$ ratio increases again to values close to 1 (0.92). The good agreement between the calculated τ values and the experimental mechanical properties also confirms that the ease with which the back-stress in the twins can be relieved is more important in determining the increase in τ_{twin} produced by particles than the Orowan stress on the twinning dislocations.

3.3. High temperature mechanical properties

Fig. 9 depicts the mechanical response of the as-extruded and the annealed bars under tension and compression along ED at 250 °C. It is apparent that the tensile curves (Fig. 9a) are concave-down and that the concave-up shape of the compressive curves (Fig. 9b) is much less pronounced than at RT, which is consistent with the typical decline of the twinning activity with increasing temperature [4,5]. Our results also show that the compressive YS of the annealed materials at 250 °C increases dramatically with respect to that of the as-extruded bar (note that, in the case of the sample annealed for 1 h, the compressive YS is even anomalously higher than that at RT), while the tensile YS at this temperature remains almost invariant for all annealing conditions (Fig. 9c). Thus,

Table 2
Relative values of the critical resolved shear stress (τ) for the as-extruded and the annealed materials.

Annealing time (h)	$\tau_{prism}/\tau'_{twin}$	τ_{pyr}/τ'_{twin}	$\tau_{basal}/\tau'_{twin}$
0	1.10	1.19	0.95
0.5	0.79	1.17	0.94
1	0.77	1.17	0.93
5	0.83	1.16	0.93
20	0.92	1.18	0.94

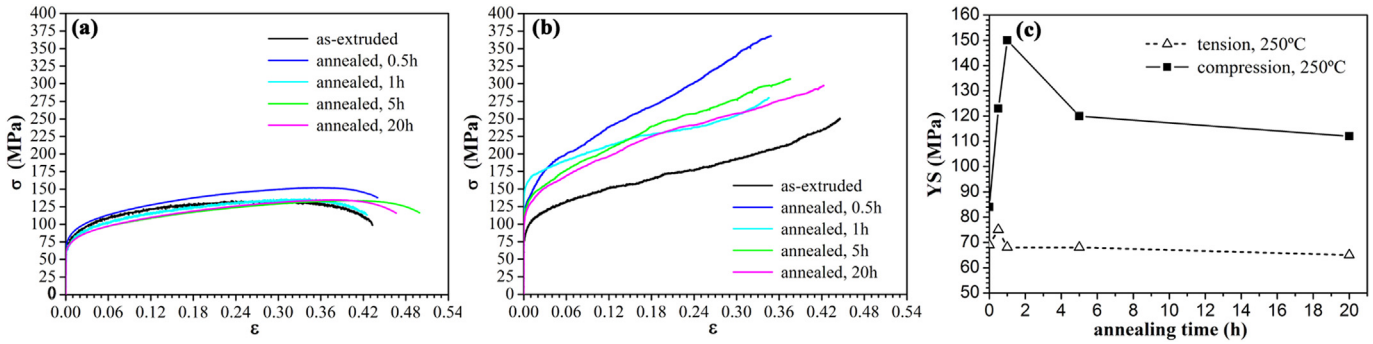

Fig. 9. Mechanical behaviour of the as-extruded and the annealed bars at 250 °C when testing along the extrusion direction: (a) tensile curves, (b) compressive curves and (c) variation of the tensile and compressive YS with the annealing time.

the reversed YS asymmetry becomes considerably more pronounced with increasing testing temperature. Similar findings have been previously reported in other weakly-textured Mg–RE alloys [34,53]. For example, the age-hardenable Mg–1.7Nd–1RE–Zn–Zr (wt.%) and Mg–8Gd–2Y–1Nd–0.3Zn–0.6Zr (wt.%) alloys displayed isotropic behaviour at RT, but were found to be stronger in compression than in tension at elevated temperature both in the as-extruded and peak-aged conditions [34], the difference depending on the grain size [53]. In the absence of twinning, whose activity declines significantly at this temperature range, the reversed YS asymmetry was attributed to varying interactions of dislocations with solute atoms and precipitates in tension and compression, but no further details were given [34]. In line with this, the high temperature reversed YS asymmetry observed earlier in the MN11 alloy by some of the present authors [35], was shown by experiments and simulations to be associated with the predominance of pyramidal <c+a> slip and with an interaction of pyramidal <c+a> dislocations with solute atoms different in tension and compression.

When <c+a> dislocations, having a very extended core, are temporarily arrested at the obstacles they continuously encounter as they move through the lattice, they try to reduce their energy by decomposition or dissociation [54–57]. Several dissociation mechanisms have been proposed. On the one hand, it has been suggested that dissociation into <c> and <a> dislocations causes the edge <c+a> dislocations to become immobile due to the fact that <c> dislocations do not move in hcp crystals. In such a situation, for the deformation to keep on propagating the cross-slip of the <c+a> screw dislocations must be thermally activated by an increment of the applied stress, which is supported by TEM studies [58–61]. On the other hand, molecular dynamic simulations have recently shown that the key <c+a> dislocations, which are metastable, could undergo a transition into various lower-energy, but immobile products lying on the basal planes, which as such serve as strong obstacles to the motion of all other dislocations [62]. Irrespectively of the exact mechanism, it is clear that the <c+a> dislocation transformations produce strengthening.

TEM examinations of samples annealed for 1 h and deformed in tension and compression at 250 °C and 10^{-3} s^{-1} up to an engineering strain of 5% (Fig. 10) appear to be consistent with a higher dissociation of <c+a> dislocations in compression. In particular, after tension (Fig. 10a), $\{11\bar{2}2\}$ and basal dislocation traces were found to be present. However, after compression (Fig. 10b), $\{11\bar{2}2\}$ dislocation traces appear to be absent, which could be interpreted as a result of the <c+a> dislocation transforming into lower-energy products lying on basal planes [54,57,62]. Moreover, after compression, one can find particles exhibiting dislocation debris on only one of their sides (see blue arrow in Fig. 10b), indicative of the lower <c+a> dislocation mobility and thus their lower ability to overcome obstacles in compression. Finally, in the compressive tested sample, some dislocations display a stepped configuration (see red arrows in Fig. 10b), usually produced by the occurrence of double cross-slip [57], which further provides evidence of the limited mobility of <c+a> dislocations in compression.

It is our contention that, possibly due to a higher hydrostatic stress in compression, the mobility of the <c+a> dislocations and thus their probability of being arrested at obstacles and/or their waiting time is higher in compression than in tension. Thus, the dissociation probability is also higher in compression than in tension, which accounts for the compressive YS being higher than the tensile YS at 250 °C.

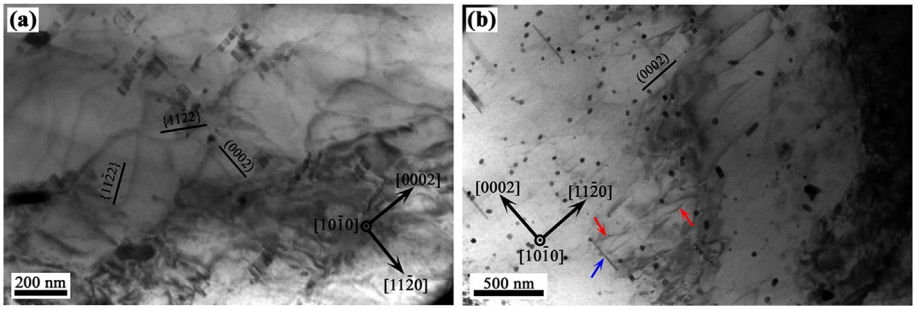

Fig. 10. TEM bright-field images of dislocations in specimens annealed for 1 h and afterwards deformed up to 5% engineering strain at 250 °C and 10^{-3} s^{-1} in (a) tension and (b) compression. The electron beam was parallel to the <10$\bar{1}$0> zone axis. The blue arrow highlights a precipitate having dislocation debris on only one side, while the red arrows highlight dislocations lines displaying a stepped configuration. (For interpretation of the references to colour in this figure legend, the reader is referred to the web version of this article.)

3.4. Outlook

Magnesium alloys are being demanded to an increasing extent in applications where the components are subjected to elevated temperatures. Therefore, great research efforts are being focused on the development of alloys that are able to withstand high stresses at high temperatures. Thorium is, due to the high thermal stability of the equilibrium phase Mg_3Th_6, the most effective alloying element known to improve significantly the high-temperature properties of magnesium [63]. However, due to its radioactivity, Th-containing alloys have been phased out and denuded efforts are being placed on replacing them. For very high-performance applications, and despite its scarcity, rare earths or similar metals have been shown to be the best option. In this way, alloys like QE22 (Mg-2.5 wt% Ag-2.1 wt% Di-0.7 wt% Zr), with a tensile YS of 205 MPa at RT, 195 MPa at 100 °C and 165 MPa at 200 °C, or the WE54 (Mg-5.2 wt% Y-3 wt.% RE-0.7 wt% Zr) and WE43 (Mg-4 wt.% Y-3.4 wt% RE-0.7 wt% Zr) alloys have been developed [23]. Our results show that the MN11 alloy, with a compressive YS ≈ 150 MPa at 250 °C, can compete with such alloys in terms of high temperature compressive strength. Since rare-earth elements are scarce, other raw materials that can exhibit a similar high temperature precipitate strengthening behaviour must be found, and the results reported in the present paper might constitute a model for the properties to be sought for.

4. Conclusions

An extruded solid solution Mg-1 wt.% Mn-1 wt.% Nd (MN11) alloy was annealed at 275 °C for different time intervals spanning from 0.5 h to 20 h in order to obtain different precipitation distributions. The mechanical behaviour of the as-extruded and the annealed materials were then characterised at room temperature and 250 °C. A transmission electron study was performed to characterise particles and their interaction with dislocations in tension and compression. The ability of the Orowan model to predict the RT strengthening produced by precipitates on the individual deformation mechanisms in the alloy was evaluated quantitatively. The following conclusions can be drawn from the present study:

1. Following annealing times as short as 0.5 h, simultaneous precipitation and dissolution of Mg_3Nd prismatic plates, with their longer axis oriented parallel to the matrix c-axis, takes place. After 5 h of annealing the volume fraction of precipitates reaches a maximum while the length of the plates reaches a minimum. Longer annealing treatments lead to a decrease of the volume fraction of precipitates due to particle dissolution and grain boundary segregation together with a simultaneous increase in their size due to coarsening.
2. Precipitation strengthens the alloy at RT, the Orowan model accounting for the hardening of the slip systems, but not fully for that of the twinning system, which is mainly determined by the stress required to relieve the additional back-stress generated by particles in the twin.
3. The strengthening effect of precipitates is anisotropic. In particular, the increment in the critical resolved shear stress is significantly higher for pyramidal <c+a> slip, twinning and basal slip than for prismatic slip. As a result, prismatic slip is strongly promoted over twinning, which leads to the appearance of reversed yield stress (YS) asymmetry at RT in the annealed samples.
4. The alloy exhibits a remarkable compressive YS at high temperature. Moreover, for specific particle distributions, an anomalous temperature dependence of the compressive YS was observed in the temperature interval ranging from room temperature to 250 °C. This causes an enhancement of the reversed YS asymmetry at high temperature.
5. The reversed YS asymmetry at high temperature appears to be associated to a different interaction of pyramidal <c+a> dislocations with solutes and particles.

Acknowledgements

Financial support from the PRI-PIBUS-2011-0917 project (MAGMAN) funded by the Spanish Ministry of Economy and Competitiveness (MINECO) is gratefully acknowledged. The research leading to these results has also received funding from Madrid Regional Government under the S2013/MIT-2775 project (DIMMAT), which is also acknowledge. In addition, one of the authors (J.D. Robson) acknowledges the financial contribution of the EPSRC via the LATEST2 programme (EP/H020047/1). The authors also thank David Pérez Risco, from CENIM, for assistance with mechanical testing, Ignacio Carabias, from the CAI Difracción de Rayos X of UCM, for assistance with XRD, David Maldonado, from IMDEA Materials Institute, for assistance with SEM and Esteban Urones, from the CNME, for assistance with TEM.

References

[1] I.J. Polmear, Magnesium alloys and applications, Mater. Sci. Tech. 10 (1994) 1–16.
[2] P.G. Partridge, The crystallography and deformation modes of hexagonal close-packed metals, Metall. Rev. 12 (1967) 169–194.
[3] S.R. Agnew, in: Advances in Wrought Magnesium Alloys. Fundamentals of Processing, Properties and Applications, first ed., Woodhead Publishing Limited, Cambridge, 2012, pp. 63–104.
[4] J.W. Christian, S. Mahajan, Deformation twinning, Prog. Mater. Sci. 39 (1995) 1–157.
[5] M.R. Barnett, in: Advances in Wrought Magnesium Alloys. Fundamentals of Processing, Properties and Applications, first ed., Woodhead Publising Limited, Cambridge, 2012, pp. 105–143.
[6] X.L. Nan, H.Y. Wang, L. Zhang, J.B. Li, Q.C. Jiang, Calculation of Schmid factors in magnesium: analysis of deformation behaviors, Scr. Mater. 67 (2012) 443–446.
[7] M.R. Barnett, A Taylor model based description of the proof stress of magnesium AZ31 during hot working, Metall. Mater. Trans. A 34 (2003) 1799–1806.
[8] H. Watanabe, K. Ishikawa, Effect of texture on high temperature deformation behavior at high strain rates in Mg-3Al-1Zn alloy, Mater. Sci. Eng. A 523 (2009) 304–311.
[9] M.R. Barnett, Z. Keshavarz, A.G. Beer, D. Atwell, Influence of grain size on the compressive deformation of wrought Mg-Al-1Zn, Acta Mater. 52 (2004) 5093–5103.
[10] A. Akhtar, E. Teghtsoonian, Solid solution strengthening of magnesium single crystals-I alloying behaviour in basal slip, Acta Metall. 17 (1969) 1339–1349.
[11] A. Akhtar, E. Teghtsoonian, Solid solution strengthening of magnesium single crystals-II the effect of solute on the ease of prismatic slip, Acta Metall. 17 (1969) 1351–1356.
[12] N. Stanford, M.R. Barnett, Solute strengthening of prismatic slip, basal slip and $\{10\bar{1}2\}$ twinning in Mg and Mg-Zn binary alloys, Int. J. Plast. 47 (2013) 165–181.
[13] J.B. Clark, Transmission electron microscopy study of age hardening in a Mg-5wt.% Zn alloy, Acta Metall. 13 (1965) 1281–1289.
[14] J.B. Clark, Age hardening in a Mg-9wt.% Al alloy, Acta Metall. 16 (1968) 141–152.
[15] M.A. Gharghouri, G.C. Weatherly, J.D. Embury, The interaction of twins and precipitates in a Mg-7.7 at.% Al alloy, Philos. Mag. 78 (1998) 1137–1149.
[16] J.F. Nie, Effects of precipitate shape and orientation on dispersion strengthening in magnesium alloys, Scr. Mater. 48 (2003) 1009–1015.
[17] N. Stanford, M.R. Barnett, Effect of particles on the formation of deformation twins in magnesium-based alloy, Mater. Sci. Eng. A 516 (2009) 226–234.
[18] J. Jain, W.J. Poole, C.W. Sinclair, M.A. Gharghouri, Reducing the tension-compression yield asymmetry in a Mg-8Al-0.5Zn alloy via precipitation, Scr. Mater. 62 (2010) 301–304.
[19] J.D. Robson, N. Stanford, M.R. Barnett, Effect of particles in promoting twin nucleation in a Mg-5 wt.% Zn alloy, Scr. Mater. 63 (2010) 823–826.
[20] J.D. Robson, N. Stanford, M.R. Barnett, Effect of precipitate shape on slip and twinning in magnesium alloys, Acta Mater. 59 (2011) 1945–1956.
[21] J. Geng, Y.B. Chun, N. Stanford, C.H.J. Davies, J.F. Nie, M.R. Barnett, Processing and properties of Mg-6Gd-1Zn-0.6Zr Part 2. Mechanical properties and particles twin interactions, Mater. Sci. Eng. A 528 (2011) 3659–3665.

[22] N. Stanford, J. Geng, Y.B. Chun, C.H.J. Davies, J.F. Nie, M.R. Barnett, Effect of plate shaped particle distributions on the deformation behaviour of magnesium alloy AZ91 in tension and compression, Acta Mater. 60 (2012) 218–228.
[23] J.F. Nie, Precipitation and hardening in magnesium alloys, Metall. Mater. Trans. A 43 (2012) 3891–3939.
[24] N. Stanford, A.S. Taylor, P. Cizek, F. Siska, M. Ramajayam, M.R. Barnett, {10$\bar{1}$2} twinning in magnesium-based lamellar microstructures, Scr. Mater. 67 (2012) 704–707.
[25] S.R. Agnew, R.P. Mulay, F.J. Polesak III, C.A. Calhoun, J.J. Bhattacharyya, B. Clausen, In situ neutron diffraction and polycrystal plasticity modeling of a Mg-Y-Nd-Zr alloy: effects of precipitation on individual deformation mechanisms, Acta Mater. 61 (2013) 3769–3780.
[26] J. Jain, P. Cizek, W.J. Poole, M.R. Barnett, Precipitate characteristics and their effect on the prismatic-slip-dominated deformation behaviour of an Mg-6Zn alloy, Acta Mater. 61 (2013) 4091–4102.
[27] V. Jain, R.S. Mishra, A.K. Gupta, Gouthama, Study of β-precipitates and their effect on the directional yield asymmetry of friction stir processed and aged AZ91C alloy, Mater. Sci. Eng. A 560 (2013) 500–509.
[28] J.D. Robson, N. Stanford, M.R. Barnett, Effect of precipitate shape and habit on mechanical asymmetry in magnesium alloys, Metall. Mater. Trans. A 44 (2013) 2984–2995.
[29] J. Wang, N. Stanford, Investigation of precipitate hardening and slip twinning in Mg5%Zn by micropillar compression, Acta Mater. 100 (2015) 53–63.
[30] J. Jain, P. Cizek, W.J. Poole, M.R. Barnett, The role of back stress caused by precipitates on {10$\bar{1}$2} twinning in a Mg-6Zn alloy, Mater. Sci. Eng. A 647 (2015) 66–73.
[31] F. Wang, J.J. Bhattacharyya, Sean R. Agnew, Effect of precipitate shape and orientation on Orowan strengthening of non-basal slip modes in hexagonal crystals, application to magnesium alloys, Mater. Sci. Eng. A 666 (2016) 114–122.
[32] S. Abaspour, C.H. Cáceres, Thermodynamic-based selection and design of creep-resistance cast Mg alloys, Metall. Mater. Trans. A 46 (2015) 5972–5988.
[33] C.L. Mendis, K.U. Kainer, N. Hort, High strength magnesium alloys through precipitation hardening and micro alloying: considerations for alloy design, JOM 67 (2015) 2427–2432.
[34] X. Hou, Z. Cao, L. Wang, S. Xu, S. Kamado, L. Wang, Microstructure and mechanical properties of extruded Mg-8Gd-2Y-1Nd-0.3Zn-0.6Zr alloy, Mater. Sci. Eng. A 528 (2011) 7805–7810.
[35] P. Hidalgo-Manrique, V. Herrera-Solaz, J. Segurado, J. Llorca, F. Gálvez, O.A. Ruano, S.B. Yi, M.T. Pérez-Prado, Origin of the reversed yield asymmetry in Mg-rare earth alloys at high temperature, Acta Mater. 90 (2015) 265–267.
[36] S. Hielscher, H. Schaeben, A novel pole figure inversión method: specification of the MTEX algorithm, J. Appl. Cryst. 41 (2008) 1024–1037.
[37] I.L. Dillamore, W.T. Roberts, Preferred orientation in wrought and annealed metals, Metall. Rev. 10 (1965) 271–380.
[38] P. Hidalgo-Manrique, S.B. Yi, J. Bohlen, D. Letzig, M.T. Pérez-Prado, Effect of Nd additions on extrusion texture development and on slip activity in a Mg-Mn alloy, Metall. Mater. Trans. A 44 (2013) 4819–4829.
[39] P. Hidalgo-Manrique, S.B. Yi, J. Bohlen, D. Letzig, M.T. Pérez-Prado, Control of the mechanical asymmetry in an extruded MN11 alloy by static annealing, Metall. Mater. Trans. A 45 (2014) 3282–3291.
[40] N. Stanford, G. Sha, J.H. Xia, S.P. Ringer, M.R. Barnett, Solute segregation and texture modification in an extruded magnesium alloy containing gadolinium, Scr. Mater 65 (2011) 919–921.
[41] J.D. Robson, Effect of rare earth additions on the texture of wrought magnesium alloys: the role of grain boundary segregation, Metall. Mater. Trans. A 45 (2014) 3205–3212.
[42] J.D. Robson, D.T. Henry, B. Davis, Particles effects on recrystallization in magnesium manganese alloys, Mater. Sci. Eng. A 528 (2011) 4239–4247.
[43] E.E. Underwood, in: Microstructural Analysis. Tools and Techniques, first ed., Plenum Press, New York-London, 1973, pp. 35–66.
[44] D.B. Williams, Carter, Transmission Electron Microscopy, second ed., Springer, New York, 2009.
[45] D. Hull, D.J. Bacon, Introduction to Dislocations, fifth ed., Butterworth-Heinemann, Oxford, 2011.
[46] A. Serra, R.C. Pond, D.J. Bacon, Computer simulation of the structure and mobility of twinning dislocations in HCP metals, Acta Metall. Mater. 39 (1991) 1469–1480.
[47] J.A. Yasi, T. Nogaret, D.R. Trinkle, Y. Qi, L.G. Hector Jr., W.A. Curtin, Basal and prism dislocation cores in magnesium: comparison of first-principles and embedded-atom-potential methods predictions, Model. Simul. Mater. Sci. Eng. 17 (2009) 055012–055013.
[48] M. Gazisaeidi, L.G. Hector Jr., W.A. Curtin, First principles core structures of <c+a> edge and screw dislocations in Mg, Scr. Mater. 75 (2014) 42–45.
[49] V. Herrera-Solaz, P. Hidalgo-Manrique, M.T. Pérez-Prado, D. Letzig, J. Llorca, J. Segurado, Effect of rare earth additions on the critical resolved shear stresses of magnesium alloys, Mater. Lett. 128 (2014) 199–203.
[50] E.A. Ball, P.B. Prangnell, Tensile-compressive yield asymmetries in high strength wrought magnesium alloys, Scr. Metall. Mater. 31 (1994) 111–116.
[51] N.M. Munroe, X. Tan, H. Gu, Orientation dependence of slip and twinning in hcp metals, Scr. Mater. 36 (1997) 1383–1386.
[52] J.D. Robson, A.M. Twier, G.W. Lorimer, P. Rogers, Effect of extrusion conditions on microstructure, texture and yield asymmetry in Mg-6Y-7Gd-0.5wt%Zr alloy, Mater. Sci. Eng. A 528 (2011) 7247–7256.
[53] C.J. Bettles, M.A. Gibson, S.M. Zhu, Microstructure and mechanical behaviour of an elevated temperature Mg-rare earth based alloy, Mater. Sci. Eng. A 505 (2009) 6–12.
[54] T. Obara, H. Yoshinaga, S. Morozumi, {11$\bar{2}$2}<$\bar{1}\bar{1}$23> slip system in magnesium, Acta Metall. 21 (1973) 845–853.
[55] M.H. Yoo, J.R. Morris, K.M. Ho, S.R. Agnew, Non basal deformation of HCP metals and alloys: role of dislocation source and mobility, Metall. Mater. Trans. A 33 (2002) 813–822.
[56] S.R. Agnew, J.A. Horton, M.H. Yoo, Transmission electron microscopy investigation of <c+a> dislocations in Mg and α-solid solution Mg-Li alloys, Metall. Mater. Trans. A 33 (2002) 851–858.
[57] J. Geng, M.F. Chisholm, R.K. Mishra, K.S. Kumar, An electron microscopy study of dislocation structures in Mg single crystals compressed along [0001] at room temperature, Philos. Mag. 95 (2015) 3910–3932.
[58] H. Tonda, S. Ando, K. Takashima, T. Vreeland Jr., Acta Metall. Mater. 42 (1994) 2845–2851.
[59] H. Tonda, S. Ando, K. Takashima, T. Vreeland Jr., Anomalous temperature dependence of the yield stress by {11$\bar{2}$2}<$\bar{1}\bar{1}$23> secondary pyramidal slip in cadmium crystals -I. Experiments, Acta Metall. Mater. 42 (1994) 2853–2858.
[60] S. Ando, H. Tonda, Non-basal slip in magnesium-lithium alloy single crystals, Mater. Trans. JIM 9 (2000) 1188–1191.
[61] H. Tonda, S. Ando, Effect of temperature and shear direction on yield stress by {11$\bar{2}$2}<$\bar{1}\bar{1}$23> slip in HCP metals, Metall. Mater. Trans. A 33 (2002) 831–836.
[62] Z. Wu, W.A. Curtin, The origins of high hardening and low ductility in magnesium, Nature 526 (2015) 62–67.
[63] B.L. Mordike, Creep-resistant magnesium alloys, Mater. Sci. Eng. A 324 (2002) 103–112.